This is a repository copy of *Room-temperature local magnetoresistance effect in n-Ge devices with low-resistive Schottky-tunnel contacts*.

White Rose Research Online URL for this paper:
https://eprints.whiterose.ac.uk/id/eprint/145140/

Version: Published Version

**Article:**

**LETTER • OPEN ACCESS**

# Room-temperature local magnetoresistance effect in *n*-Ge devices with low-resistive Schottky-tunnel contacts

To cite this article: Makoto Tsukahara *et al* 2019 *Appl. Phys. Express* **12** 033002

View the article online for updates and enhancements.

**LETTER**

# Room-temperature local magnetoresistance effect in *n*-Ge devices with low-resistive Schottky-tunnel contacts

Makoto Tsukahara[1], Michihiro Yamada[1], Takahiro Naito[1], Shinya Yamada[1,2], Kentarou Sawano[3], Vlado K. Lazarov[4], and Kohei Hamaya[1,2*]

[1]Graduate School of Engineering Science, Osaka University, 1-3 Machikaneyama, Toyonaka 560-8531, Japan
[2]Center for Spintronics Research Network, Osaka University, 1-3 Machikaneyama, Toyonaka 560-8531, Japan
[3]Advanced Research Laboratories, Tokyo City University, 8-15-1 Todoroki, Tokyo 158-0082, Japan
[4]Department of Physics, University of York, York YO10 5DD, United Kingdom

*E-mail: hamaya@ee.es.osaka-u.ac.jp

Two-terminal local magnetoresistance (MR) effect in *n*-type germanium (Ge) based lateral spin-valve (LSV) devices can be observed at room temperature. By using phosphorus $\delta$-doped Heusler-alloy/Ge Schottky-tunnel contacts, the resistance-area product of the contacts is able to be less than 0.20 k$\Omega$ $\mu m^2$, which is the lowest value in semiconductor based LSV devices. From the one-dimensional spin drift-diffusion model, the interface spin polarization of the Heusler-alloy/Ge contacts in the present LSV devices can be estimated to be ~0.018 at room temperature. We experimentally propose that it is important for enhancing the local MR ratio in *n*-Ge based LSV devices to improve the interface spin polarization of the Heusler-alloy/Ge contacts. © 2019 The Japan Society of Applied Physics

For developing semiconductor-based spintronic applications,[1–7] electrical spin injection and detection techniques have been explored in III–V[8] and group-IV[9–11] semiconductors. In general, four-terminal nonlocal voltage measurements in lateral spin-valve (LSV) devices[12–14] have been utilized as evidence for spin transport in nonmagnetic materials. In this scheme, since the precession of the spin angular momentum can be electrically detected by applying perpendicular magnetic fields to the polarized spins even in semiconductor channel layers,[8,10,11] it has been recognized that the four-terminal nonlocal Hanle-effect curves in both parallel and anti-parallel magnetization states are the most reliable evidence for the spin transport in semiconductors. So far, only a few studies have clearly shown the nonlocal Hanle-effect curves at room temperature in both parallel and anti-parallel magnetization states for Si[15–17] and Ge[18] although only room-temperature nonlocal spin signals (not Hanle-effect curves) have been shown for GaAs.[19–22]

In general, two-terminal local magnetoresistance (MR) measurements have also been utilized to examine spin-dependent transport of spin-polarized electrons or holes through semiconductors.[23–30] Recent studies of GaAs-based LSV devices showed large MR ratio from 10% to 50% but the data were limited at low temperatures.[31,32] To explore the possibility of the novel applications to Si-based conventional complementary metal-oxide-semiconductor (CMOS) transistors with the nonvolatile memory functionality, the two-terminal MR effect in *n*-Si has also been examined even at room temperature.[33–37] On the other hand, there is no report on the two-terminal local MR effect in *n*-Ge at room temperature despite a next generation channel material for CMOS transistors.[38,39]

In this letter, using *n*-Ge LSV devices with phosphorus (P) $\delta$-doped Heusler-alloy/Ge Schottky-tunnel contacts, we observe the two-terminal local MR effect at room temperature. In these LSV devices, the resistance-area product (*RA*) of the contacts is able to be less than 0.20 k$\Omega$ $\mu m^2$, which is the

lowest value in semiconductor based LSV devices. From the one-dimensional spin drift-diffusion model, the interface spin polarization of the Heusler-alloy/Ge contacts can be estimated to be ~0.018 at room temperature. For enhancing the local MR ratio in *n*-Ge based LSV devices, it is important to improve the interface spin polarization of the Heusler-alloy/Ge contacts.

The following is the device fabrication procedure. By means of molecular beam epitaxy (MBE), we first grew an undoped Ge(111) layer (~28 nm) at 350 °C (LT-Ge) on the commercial undoped Si(111) substrate ($\rho \sim 1000\,\Omega$ cm). Then, an undoped Ge(111) layer (~70 nm) was grown at 700 °C (HT-Ge) on top of the LT-Ge.[40] As the spin-transport layer, we grew a 140 nm thick P-doped *n*-Ge(111) layer (doping concentration $\sim 10^{19}$ cm$^{-3}$) by MBE at 350 °C on top of the HT-Ge layer. The carrier concentration ($n$) in the *n*-Ge(111) layer was estimated to be $n \sim 1 \times 10^{19}$ cm$^{-3}$ at room temperature by Hall effect measurements. To promote the tunneling conduction of electron spins through the Schottky barriers,[41–43] a P $\delta$-doped Ge layer ($n^+$-Ge) with an ultra-thin Si insertion layer was grown on top of the spin-transport layer.[44] As a spin injector and detector, we used Co$_2$FeAl (CFA), expected to have a relatively high spin polarization,[45,46] grown by low-temperature MBE.[18] Detailed growth procedures have been published elsewhere.[47,48] Figure 1(a) shows a schematic diagram of an LSV device fabricated for two-terminal local and four-terminal nonlocal measurements. For controlling two-different magnetization states between parallel and anti-parallel, the two-different CFA/*n*-Ge contacts with $0.4 \times 5.0$ $\mu m^2$ (FM1) and $1.0 \times 5.0$ $\mu m^2$ (FM2) were fabricated by conventional electron-beam lithography and Ar-ion milling.[48–50] The edge-to-edge distance, *d*, between the CFA/*n*-Ge contacts was ~0.4 $\mu m$.

Figure 1(b) displays an atomic resolution high angle annular dark field scanning transmission electron microscopy image of the CFA/*n*-Ge interface in an LSV device. Because of the $\delta$-doping near the interface, a few atomic layers (~5 Å)

© 2019 The Japan Society of Applied Physics

(a)



(b) Co₂FeAl

(c)
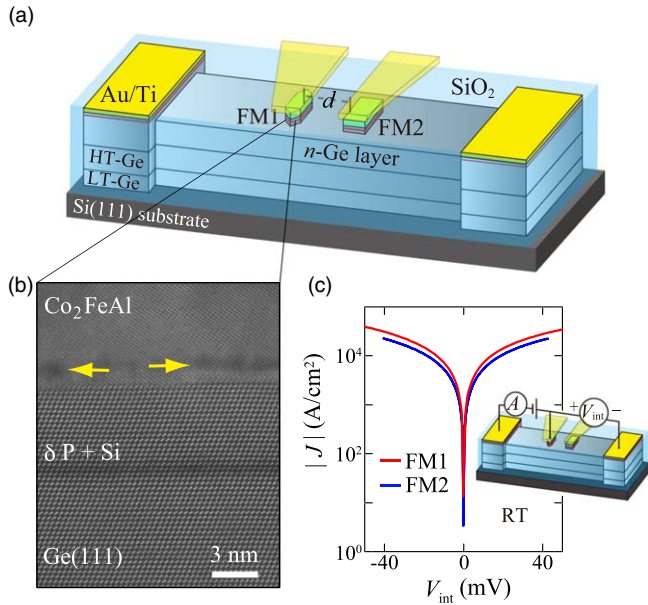


**Fig. 1.** (Color online) (a) Schematic diagram of an LSV device with Co₂FeAl/$n^+$-Ge contacts for both four-terminal and two-terminal magnetoresistance measurements. (b) HAADF STEM image of the Co₂FeAl/$n^+$-Ge interface of a contact in an LSV device. (c) $|J|$–$V$ curves of the Co₂FeAl/$n^+$-Ge contacts (FM1 and FM2) at 296 K.

of P + Si insertion can be seen. We note that there is some fluctuation of the atomic composition in the CFA layer near the interface, as denoted by yellow arrows. In our recent work on Co₂FeAl₀.₅Si₀.₅ (CFAS)/$n$-Ge interface, we found that the Ge atoms in the $\delta$-doped layer are outdiffusing in the CFAS layer,[51] leading to the same fluctuation of the atomic composition near the interface. We will present in the last paragraph some discussion about the influence of the atomic composition fluctuation in the CFA/$n$-Ge interface. Owing to the $\delta$-doping near the interface, the current density–voltage ($|J|$–$V$) characteristics of the CFA/$n$-Ge contacts show almost no rectifying behavior at room temperature [Fig. 1(c)], which indicates the demonstration of the tunneling conduction of electrons through the CFA/$n$-Ge interfaces. Here the $|J|$–$V$ characteristics were measured by the three-terminal measurements, as depicted in the inset of Fig. 1(c). From these measurements, the $RA$ value of the CFA/$n$-Ge contacts can be estimated to be 0.12–0.34 kΩ μm² at 296 K, one order of magnitude larger than the spin resistance of the grown $n$-Ge spin transport layer (∼0.014 kΩ μm² at 296 K). Note that the Schottky barrier height of Heusler alloy/$n$-Ge(111) junctions is relatively low (0.4–0.5 eV)[52] compared to Heusler alloy/$n$-GaAs ones and the barrier width can be intentionally reduced by developing an original $\delta$-doping technique near the interface.[44] As a result, the $RA$ value of less than ∼0.20 kΩ μm² is the lowest value in semiconductor based LSV devices reported so far, meaning an advantage of achieving low power consumption devices.

For these LSV devices with the low-$RA$ Schottky-tunnel contacts, we measured spin transport in $n$-Ge, where the measurement schemes of the two-terminal local and four-terminal nonlocal methods were depicted in Fig. 2(a). Figures 2(b) and 2(c) show representative four-terminal nonlocal spin signals ($\Delta R_{NL} = \Delta V_{NL}/I$) at 200 K and 296 K, respectively, by sweeping in-plane magnetic fields ($B_y$) at $I = -2.0$ mA, where the negative sign of $I$ ($I < 0$)

(a)



(b) $T = 200$ K     (c) $T = 296$ K



(d) $T = 200$ K     (e) $T = 296$ K
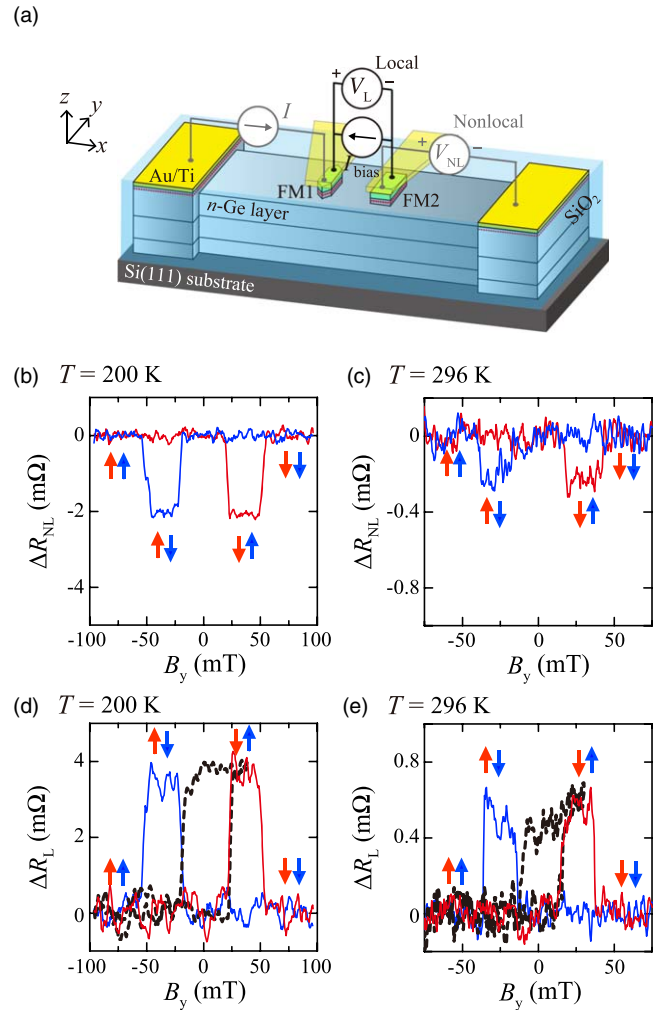


**Fig. 2.** (Color online) (a) Terminal configurations of four-terminal nonlocal and two-terminal local magnetoresistance measurements in $n$-Ge based LSV devices. Nonlocal magnetoresistance curves at (b) 200 K at $I = -2.0$ mA and (c) 296 K at $I = -2.0$ mA. Local magnetoresistance curves at (d) 200 K at $I_{bias} = -2.0$ mA and (e) 296 K at $I_{bias} = -3.5$ mA. The black dashed curves are minor loops.

indicates that the spin-polarized electrons are injected into the $n$-Ge layer from CFA, i.e., spin injection condition via the Schottky-tunnel barrier. Although the amplitude of $\Delta R_{NL}$ is decreased by elevating the external temperature from 200 to 296 K, the hysteretic nature depends on the parallel and anti-parallel magnetization states between FM1 and FM2 (see the arrows in the figures). By sweeping perpendicular magnetic fields ($B_z$), we also confirmed nonlocal Hanle-effect curves at room temperature in both parallel and anti-parallel magnetization states at 200 and 296 K (not shown here), as clearly shown in our previous works.[18,48–50]

Using the same LSV devices, we recorded two-terminal local spin signals ($\Delta R_L = \Delta V_L/I_{bias}$) at 200 K and 296 K, as presented in Figs. 2(d) and 2(e), respectively, at bias currents of $I_{bias} = -2.0$ mA and $-3.5$ mA. Evident positive $\Delta R_L$ changes with hysteretic nature can also be observed even at room temperature. Here we also measured minor-loop data (see black dashed curves) in the same figures, meaning that the anti-parallel magnetization state between FM1 and FM2 is stable and positive $\Delta R_L$ changes are attributed to the spin-dependent transport of electrons through the $n$-Ge layer. In Fig. 2(e) we can understand that a reliable local MR effect up to room temperature is detected even in an $n$-Ge LSV device.

From these data, the MR ratio (%), $(\Delta R_{\mathrm{L}}/R_{\mathrm{P}})\times100$, can be estimated to be about 0.002% and $\sim$0.001% at 200 K and 296 K, respectively, where $R_{\mathrm{P}}$ is the resistance in the parallel magnetization state in the LSV devices used. A typical value of $R_{\mathrm{P}}$ is $\sim$100 $\Omega$, where the interface resistance at the two CFA/$n$-Ge contacts is dominant ($\sim$80 $\Omega$). Although the estimated MR ratios are extremely small as well as the reported Si LSV devices,[33,34,37] this is a first step for room-temperature applications with $n$-Ge on the Si platform.

These features were reproduced in lots of LSV devices fabricated in our processes. To understand the extremely small MR ratio in the two-terminal measurements, we roughly consider the values of $\Delta R_{\mathrm{L}}/R_{\mathrm{P}}$ obtained for various LSV devices. According to the standard theory based on the one-dimensional spin drift-diffusion model by Ref. 53 the magnitude of $\Delta R_{\mathrm{L}}$ and $R_{\mathrm{p}}$ in ferromagnet(FM)/semiconductor(SC)/ferromagnet with double tunnel barriers has been expressed as follows[34,53–56]

$$\Delta R_{\mathrm{L}} = \frac{8\gamma^2 r_{\mathrm{b}}^2 r_{\mathrm{N}}}{\left[(2r_{\mathrm{b}}+r_{\mathrm{N}})^2\exp\left(\frac{d}{\lambda_{\mathrm{N}}}\right)-r_{\mathrm{N}}^2\exp\left(-\frac{d}{\lambda_{\mathrm{N}}}\right)\right]S_{\mathrm{N}}}, \quad (1)$$

$$R_{\mathrm{p}} = \frac{1}{S_{\mathrm{N}}}\left[r_{\mathrm{N}}\frac{d}{\lambda_{\mathrm{N}}} + 2(1-\gamma^2)r_{\mathrm{b}} + 2\frac{\gamma^2 r_{\mathrm{N}} r_{\mathrm{b}}\tanh\left(\frac{d}{2\lambda_{\mathrm{N}}}\right)}{r_{\mathrm{b}}+r_{\mathrm{N}}\tanh\left(\frac{d}{2\lambda_{\mathrm{N}}}\right)}\right], \quad (2)$$

where $\gamma$ is the spin polarization of the FM/SC interfaces, $r_{\mathrm{b}}$ is regarded as the value of $RA$ measured by the three-terminal voltage measurement for the FM/SC contacts, as shown in the inset of Fig. 1(c), $S_{\mathrm{N}}$ is the cross sectional area of the SC spin-transport channel ($S_{\mathrm{N}} = 0.98 \ \mu\mathrm{m}^2$). $\lambda_{\mathrm{N}}$ and $r_{\mathrm{N}}$ ($=\rho_{\mathrm{N}}\times\lambda_{\mathrm{N}}$) are the spin diffusion length and the spin resistance of the SC layer, respectively. Considering this relation, one can expect the correlation between $\Delta R_{\mathrm{L}}/R_{\mathrm{P}}$ and $r_{\mathrm{b}}/r_{\mathrm{N}}$, as already described in Ref. 54.

In Fig. 3 we plot $\Delta R_{\mathrm{L}}/R_{\mathrm{P}}$ versus $r_{\mathrm{b}}/r_{\mathrm{N}}$ at various temperatures and show the theoretical curves based on Eqs. (1) and (2), where $d = 0.4 \ \mu\mathrm{m}$, $\lambda_{\mathrm{N}} = 0.44$ (296 K)–0.60 (150 K) $\mu\mathrm{m}$, estimated from the some experiments in our previous reports[18,48–50] and $\rho_{\mathrm{N}} = 3.1$ (296 K) $- 2.7$ (150 K) m$\Omega$ cm, measured by a four-point probe method for the devices used here. As a reference, we also indicated the value of $RA$ at 296 K in the upper horizontal axis in Fig. 3. Here, we named the LSV devices having different $RA$ ($=r_{\mathrm{b}}$) values as Device A–Device I. For Device A, B, C, and D, only the data at 296 K were plotted while the data from 150 to 296 K were shown for Device E, F, G, and H. Also, two data at 150 and 200 K can be reliably observed for Device I. It should be noted that we could not observe clear local MR signals at room temperature due to the large electrical noise while the nonlocal MR ones could be observed for high-$RA$ ($>$1.0 k$\Omega$ $\mu\mathrm{m}^2$) devices. The values of $r_{\mathrm{b}}$ and $r_{\mathrm{N}}$ are ranging from 0.11 to 3.9 k$\Omega$ $\mu\mathrm{m}^2$ and from 0.013 to 0.017 k$\Omega$ $\mu\mathrm{m}^2$, respectively. As consequences, $\Delta R_{\mathrm{L}}/R_{\mathrm{P}}$ values at 296 K are less than $10^{-5}$, i.e., MR ratios are still less than 0.001%. Also, the experimental data at 296 K can quantitatively be reproduced by the theoretical curve with $\gamma = 0.018$. This means that the interface spin polarization of the CFA/$n$-Ge contacts in this study is approximately 1.8% at room
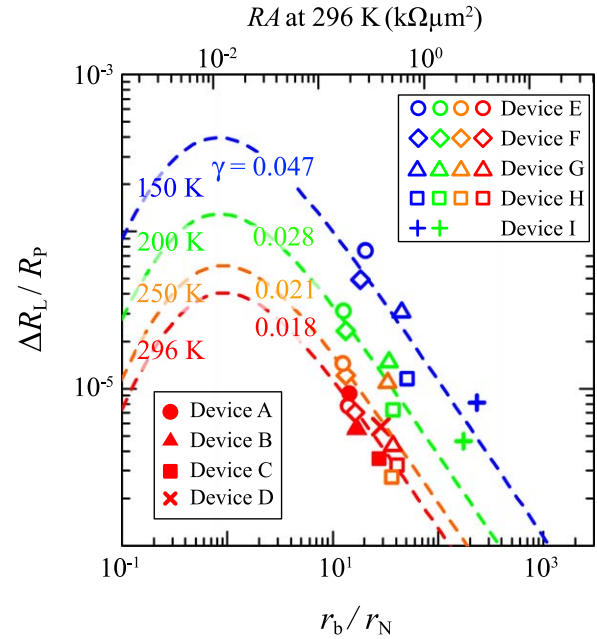


**Fig. 3.** (Color online) $\Delta R_{\mathrm{L}}/R_{\mathrm{P}}$ versus $r_{\mathrm{b}}/r_{\mathrm{N}}$ of various Co$_2$FeAl/$n$-Ge LSV devices. The dashed curves are theoretical curves based on Eqs. (1) and (2).

temperature. This value is the same order of magnitude for the spin injection/detection efficiency ($\sim$1%) estimated from the four-terminal nonlocal measurements at room temperature.[18] In the same nonlocal measurements, we have already observed the enhancement in the spin injection/detection efficiency up to 6%–9% for CFAS/$n$-Ge contacts at low temperatures.[7,51] Thus, if we also analyzed the local MR data at low temperatures, the enhancement in the MR ratio based on the increase in the value of $\gamma$ can be expected. Indeed, the value of $\gamma$, estimated from the local MR data, can be increased with decreasing external temperature. At 150 K, the MR ratio and the $\gamma$ value are approximately 0.007% and 0.047 (4.7%), respectively. Accordingly, we experimentally clarify that the value of the MR ratio in $n$-Ge based LSV devices is dominated by the value of interface spin polarization, $\gamma$.

We discuss important aspects to demonstrate large MR ratios in $n$-Ge based spintronic applications. In this study, we now clarified that the MR ratios depend experimentally on the interface spin polarization, $\gamma$, by examining temperature dependence of $\Delta R_{\mathrm{L}}/R_{\mathrm{P}}$, as shown in Fig. 3. Although such expectations have so far been reported by theorists,[53–55] there are few experimental demonstrations of systematic studies of MR ratios in the field of semiconductor spintronics. In Fig. 3 we have demonstrated low $RA$ values of less than $\sim$0.20 k$\Omega$ $\mu\mathrm{m}^2$, leading to the relatively low $r_{\mathrm{b}}/r_{\mathrm{N}}$ values. Whereas further low $RA$ values of $\sim$0.01 k$\Omega$ $\mu\mathrm{m}^2$ are optimum condition for observing large MR ratios,[53–55] the spin absorption at the FM/Ge contacts on the spin transport might affect.[57] Thus, it is more important for enhancing the MR ratio to increase $\gamma$ than to reduce $r_{\mathrm{b}}/r_{\mathrm{N}}$. As a possible and realistic issue, we should further explore methods for the increase in $\gamma$ in the present $r_{\mathrm{b}}/r_{\mathrm{N}}$ range.

In particular, the following two factors should be considered in our $n$-Ge LSV structures. First, it has been proposed that the quality of the FM/SC interface is one of the most important factor to achieve high spin injection efficiency in semiconductor spintronic devices.[58] As shown

in Fig. 1(b), because there is some fluctuation of the atomic composition in the CFA layer near the interface, we can recognize that the bulk spin polarization of the CFA film near the interface is not so high. Actually, the magnetic moment of the CFA film grown on Ge(111) was reduced to be about 90% of the CFA bulk[48] and it was caused by the outdiffusion of the Ge atoms from the $\delta$-doped layer.[51] To enhance the value of $\gamma$ of the CFA/$n$-Ge contacts, further improvements of the growth condition of Heusler alloys such as CFA on Ge(111) should be explored in detail. Next, in some of Heusler/MgO/Heusler magnetic tunnel junctions, it has been proposed that interfacial noncollinear magnetic structures at higher temperatures can affect the reduction in the spin-dependent tunneling of electrons.[59] Since the value of $\gamma$ depended on the external temperature, as shown in Fig. 3, we should also consider the interfacial exchange stiffness constant of Heusler/Ge heterointerfaces to exactly improve the value of $\gamma$. From these considerations, the results of this study will propose experimentally important aspects for achieving high-performance semiconductor spintronic applications.

In summary, we have observed two-terminal local MR effect in $n$-Ge based LSV devices at room temperature. By using P $\delta$-doped Heusler-alloy/Ge Schottky-tunnel contacts, the $RA$ value of the contacts was able to be less than $0.20\,\mathrm{k\Omega}\ \mu\mathrm{m}^2$, which is the lowest value in semiconductor based LSV devices. However, the room-temperature MR ratio was still extremely low, which is less than 0.001%. From the one-dimensional spin drift-diffusion model, the interface spin polarization of the Heusler-alloy/Ge contacts was estimated to be $\sim0.018$ at room temperature. We propose that it is important for enhancing the local MR ratio in $n$-Ge based LSV devices to improve the interface spin polarization of the Heusler-alloy/Ge contacts.

1) I. Žutić, J. Fabian, and S. D. Sarma, Rev. Mod. Phys. **76**, 323 (2004).
2) M. Tanaka and S. Sugahara, IEEE Trans. Electron Devices **54**, 961 (2007).
3) H. Dery, P. Dalal, Ł. Cywiński, and L. J. Sham, Nature **447**, 573 (2007).
4) A. M. Bratkovsky, Rep. Prog. Phys. **71**, 026502 (2008).
5) R. Jansen, Nat. Mater. **11**, 400 (2012).
6) M. Ciorga, J. Phys.: Condens. Matter **28**, 453003 (2016).
7) K. Hamaya, Y. Fujita, M. Yamada, M. Kawano, S. Yamada, and K. Sawano, J. Phys. D: Appl. Phys. **51**, 393001 (2018).
8) X. Lou, C. Adelmann, S. A. Crooker, E. S. Garlid, J. Zhang, K. S. M. Reddy, S. D. Flexner, C. J. Palmstrøm, and P. A. Crowell, Nat. Phys. **3**, 197 (2007).
9) I. Appelbaum, B. Huang, and D. J. Monsma, Nature **447**, 295 (2007).
10) O. M. J. van't Erve, A. T. Hanbicki, M. Holub, C. H. Li, C. Awo-Affouda, P. E. Thompson, and B. T. Jonker, Appl. Phys. Lett. **91**, 212109 (2007).
11) Y. Zhou, W. Han, L.-T. Chang, F. Xiu, M. Wang, M. Oehme, I. A. Fischer, J. Schulze, R. K. Kawakami, and K. L. Wang, Phys. Rev. B **84**, 125323 (2011).
12) M. Johnson and R. H. Silsbee, Phys. Rev. Lett. **55**, 1790 (1985).
13) F. J. Jedema, H. B. Heersche, A. T. Filip, J. J. A. Baselmans, and B. J. van Wees, Nature **416**, 713 (2002).
14) T. Kimura and Y. Otani, J. Phys.: Condens. Matter **19**, 165216 (2007).
15) T. Suzuki, T. Sasaki, T. Oikawa, M. Shiraishi, Y. Suzuki, and K. Noguchi, Appl. Phys. Express **4**, 023003 (2011).
16) M. Ishikawa, T. Oka, Y. Fujita, H. Sugiyama, Y. Saito, and K. Hamaya, Phys. Rev. B **95**, 115302 (2017).
17) A. Spiesser, H. Saito, Y. Fujita, S. Yamada, K. Hamaya, S. Yuasa, and R. Jansen, Phys. Rev. Appl. **8**, 064023 (2017).
18) M. Yamada, M. Tsukahara, Y. Fujita, T. Naito, S. Yamada, K. Sawano, and K. Hamaya, Appl. Phys. Express **10**, 093001 (2017).
19) G. Salis, A. Fuhrer, R. R. Schlittler, L. Gross, and S. F. Alvarado, Phys. Rev. B **81**, 205323 (2010).
20) T. Uemura, T. Akiho, M. Harada, K. Matsuda, and Y. Yamamoto, Appl. Phys. Lett. **99**, 082108 (2011).
21) T. Saito, N. Tezuka, M. Matsuura, and S. Sugimoto, Appl. Phys. Express **6**, 103006 (2013).
22) T. A. Peterson, S. J. Patel, C. C. Geppert, K. D. Christie, A. Rath, D. Pennachio, M. E. Flatté, P. M. Voyles, C. J. Palmstrøm, and P. A. Crowell, Phys. Rev. B **94**, 235309 (2016).
23) R. Mattana, J.-M. George, H. Jaffrès, F. Nguyen Van Dau, A. Fert, B. Lépine, A. Guivar'ch, and G. Jézéquel, Phys. Rev. Lett. **90**, 166601 (2003).
24) J. Moser et al., Appl. Phys. Lett. **89**, 162106 (2006).
25) K. Hamaya et al., Phys. Rev. B **77**, 081302(R) (2008).
26) I. Muneta, S. Ohya, and M. Tanaka, Appl. Phys. Lett. **100**, 162409 (2012).
27) P. Bruski, Y. Manzke, R. Farshchi, O. Brandt, J. Herfort, and M. Ramsteiner, Appl. Phys. Lett. **103**, 052406 (2013).
28) N. Matsuo, N. Doko, T. Takada, H. Saito, and S. Yuasa, Phys. Rev. Appl. **6**, 034011 (2016).
29) M. Kawano, M. Ikawa, K. Santo, S. Sakai, H. Sato, S. Yamada, and K. Hamaya, Phys. Rev. Mater. **1**, 034604 (2017).
30) M. Yamada, T. Naito, M. Tsukahara, S. Yamada, K. Sawano, and K. Hamaya, Semicond. Sci. Technol. **33**, 114009 (2018).
31) M. Oltscher, F. Eberle, T. Kuczmik, A. Bayer, D. Schuh, D. Bougeard, M. Ciorga, and D. Weiss, Nat. Commun. **8**, 1807 (2017).
32) H. Asahara, T. Kanaki, S. Ohya, and M. Tanaka, Appl. Phys. Exp. **11**, 033003 (2018).
33) T. Sasaki, T. Oikawa, T. Suzuki, M. Shiraishi, Y. Suzuki, and K. Noguchi, Appl. Phys. Lett. **98**, 262503 (2011).
34) Y. Saito, T. Tanamoto, M. Ishikawa, H. Sugiyama, T. Inokuchi, K. Hamaya, and N. Tezuka, J. Appl. Phys. **115**, 17C514 (2014).
35) T. Sasaki, Y. Ando, M. Kameno, T. Tahara, H. Koike, T. Oikawa, T. Suzuki, and M. Shiraishi, Phys. Rev. Appl. **2**, 034005 (2014).
36) T. Tahara, Y. Ando, M. Kameno, H. Koike, K. Tanaka, S. Miwa, Y. Suzuki, T. Sasaki, T. Oikawa, and M. Shiraishi, Phys. Rev. B **93**, 214406 (2016).
37) M. Ishikawa, M. Tsukahara, M. Yamada, Y. Saito, and K. Hamaya, IEEE Trans. Magn. **54**, 11 (2018).
38) D. Kuzum, A. J. Pethe, T. Krishnamohan, and K. C. Saraswat, IEEE Trans. Electron Devices **56**, 648 (2009).
39) A. Toriumi and T. Nishimura, Jpn. J. Appl. Phys. **57**, 010101 (2018).
40) K. Sawano, Y. Hoshi, S. Kudo, K. Arimoto, J. Yamanaka, K. Nakagawa, K. Hamaya, M. Miyao, and Y. Shiraki, Thin Solid Films **613**, 24 (2016).
41) Y. Ando, K. Hamaya, K. Kasahara, Y. Kishi, K. Ueda, K. Sawano, T. Sadoh, and M. Miyao, Appl. Phys. Lett. **94**, 182105 (2009).
42) K. Kasahara, Y. Baba, K. Yamane, Y. Ando, S. Yamada, Y. Hoshi, K. Sawano, M. Miyao, and K. Hamaya, J. Appl. Phys. **111**, 07C503 (2012).
43) K. Kasahara, Y. Fujita, S. Yamada, K. Sawano, M. Miyao, and K. Hamaya, Appl. Phys. Express **7**, 033002 (2014).
44) M. Yamada, K. Sawano, M. Uematsu, and K. M. Itoh, Appl. Phys. Lett. **107**, 132101 (2015).
45) W. Wang, H. Sukegawa, R. Shan, S. Mitani, and K. Inomata, Appl. Phys. Lett. **95**, 182502 (2009).
46) Z. Wen, H. Sukegawa, S. Kasai, M. Hayashi, S. Mitani, and K. Inomata, Appl. Phys. Express **5**, 063003 (2012).
47) S. Yamada, K. Tanikawa, S. Oki, M. Kawano, M. Miyao, and K. Hamaya, Appl. Phys. Lett. **105**, 071601 (2014).
48) Y. Fujita, M. Yamada, M. Tsukahara, T. Oka, S. Yamada, T. Kanashima, K. Sawano, and K. Hamaya, Phys. Rev. Appl. **8**, 014007 (2017).
49) Y. Fujita, M. Yamada, S. Yamada, T. Kanashima, K. Sawano, and K. Hamaya, Phys. Rev. B **94**, 245302 (2016).
50) M. Yamada, Y. Fujita, M. Tsukahara, S. Yamada, K. Sawano, and K. Hamaya, Phys. Rev. B **95**, 161304(R) (2017).
51) B. Kuerbanjiang et al., Phys. Rev. B **98**, 115304 (2018).
52) K. Yamane, K. Hamaya, Y. Ando, Y. Enomoto, K. Yamamoto, T. Sadoh, and M. Miyao, Appl. Phys. Lett. **96**, 162104 (2010).
53) A. Fert and H. Jaffrès, Phys. Rev. B **64**, 184420 (2001).
54) A. Fert, J.-M. George, H. Jaffrès, and R. Mattana, IEEE Trans. Electron Devices **54**, 921 (2007).
55) H. Jaffrès, J.-M. George, and A. Fert, Phys. Rev. B **82**, 140408(R) (2010).
56) P. Laczkowski, L. Vila, V.-D. Nguyen, A. Marty, J.-P. Attané, H. Jaffrès, J.-M. George, and A. Fert, Phys. Rev. B **85**, 220404(R) (2012).
57) M. Yamada, Y. Fujita, S. Yamada, K. Sawano, and K. Hamaya, Materials **11**, 150 (2018).
58) T. J. Zega, A. T. Hanbicki, S. C. Erwin, I. Žutić, G. Kioseoglou, C. H. Li, B. T. Jonker, and R. M. Stroud, Phys. Rev. Lett. **96**, 196101 (2006).
59) Y. Miura, K. Abe, and M. Shirai, Phys. Rev. B **83**, 214411 (2011).